Chemical surface tuning electrocatalysis of redox-active nanoparticles

Zhu, Nan; Ulstrup, Jens; Chi, Qijin

Publication date:
2012

Document Version
Publisher's PDF, also known as Version of record

Chemical Surface Tuning Electrocatalysis of Redox-active Nanoparticles in Two-dimensional Assembly

Nan Zhu, Jens Ulstrup, Qijin Chi *

Department of Chemistry and NanoDTU, Technical University of Denmark, DK-2800 Kgs. Lyngby, Denmark. (E-mail: cq@kemi.dtu.dk)*

Abstract This work focuses on electron transfer (ET) and electrocatalysis of inorganic hybrid *Prussian blue* nanoparticles (PBNPs, 6 nm) immobilized on different chemical surfaces. Through surface self-assembly chemistry, we have enabled to tune chemical properties of the electrode surface. Stable immobilization of the PBNPs on Au(111) surfaces modified by self-assembled monolayers (SAMs) with various terminal groups including positively charged groups ($-NH_3^+$), negatively charged groups ($-COO^-$), and neutral and hydrophobic groups ($-CH_3$) has been achieved. The surface microscopic structures of immobilized PBNPs are characterized by atomic force microscopy (AFM). Reversible electron transfer (ET) was detected by cyclic voltammetry (CV) of the PBNPs on all the surfaces. ET kinetics can be controlled by adjusting the chain length of the SAMs. The rate constants are found to depend exponentially on the ET distance, with a decay factor (β) of ca. 0.9, 1.1, 1.3 per CH_2, respectively. This feature suggests a tunneling mechanism adopted by the nanoparticles, resembling that for metalloproteins in a similar assembly. High-efficient electrocatalysis towards the reduction of H_2O_2 is observed, and possible catalytic mechanisms are discussed.

Two-dimensional Surface Self-assembly

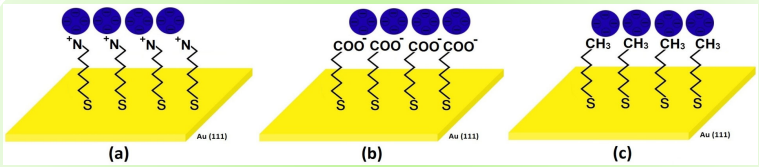

Schematic diagrams of assembling PBNPs on different chemical surfaces: (a) $NH_2(CH_2)_nS$-Au(111); (b) $HOOC(CH_2)_nS$-Au(111), and (c) $CH_3(CH_2)_nS$-Au(111).

Controlling Electron Transfer Kinetics

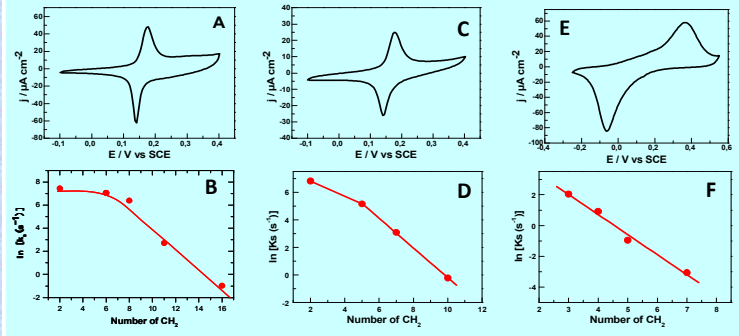

Top: Cyclic voltammograms (CVs) of (A) PBNPs-$NH_2(CH_2)_6S$-Au(111); (C) PBNPs-$OOC(CH_2)_5S$-Au(111), and (E) PBNPs-$CH_3(CH_2)_5S$-Au(111) obtained in 0.1 M KCl with the same scan rate of 0.5 V s^{-1}.

Bottom: The dependence of apparent rate constants on the distance denoted by the number of -CH_2- units

(B) PBNPs-$NH_2(CH_2)_nS$-Au(111), gives rise to a decay factor (β) of ca. 0.9 per CH_2 (i.e., equivalent to ca. 0.7 $Å^{-1}$).

(D) PBNPs-$OOC(CH_2)_nS$-Au(111), a decay factor (β) of ca. 1.1 per CH_2.

(F) PBNPs-$CH_3(CH_2)_nS$-Au(111), a decay factor (β) of ca. 1.3 per CH_2.

Chemical Surface Tuning Electrocatalysis

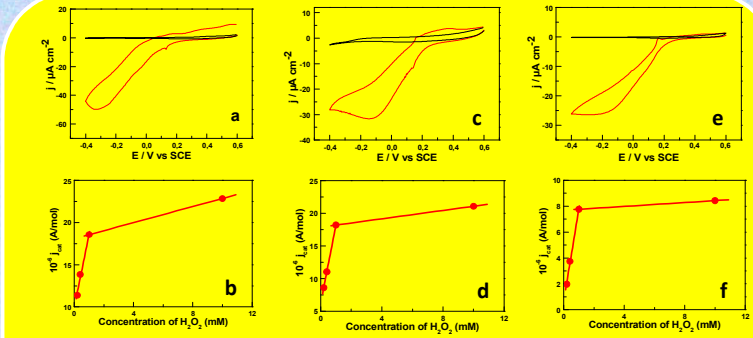

Comparison of electrocatalytic activity towards reduction of H_2O_2 with (red) or without PBNPs (black) and calibration plots of electrocatalytic activity towards different concentrations of H_2O_2 for (a) and (b) $NH_2(CH_2)_6S$-Au(111); (c) and (d) $HOOC(CH_2)_5S$-Au(111); (e) and (f) $CH_3(CH_2)_5S$-Au(111) in 0.1 M KCl. Scan rate: 20 mV s^{-1}.

Surface Structure and Size of PBNPs

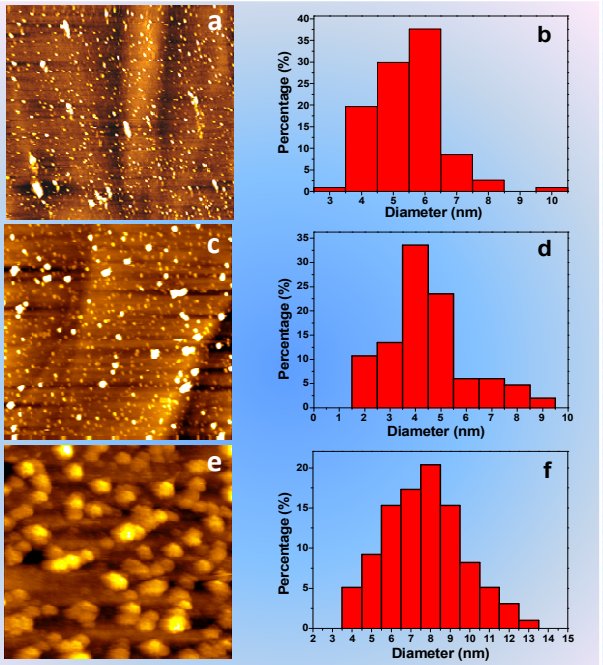

AFM images and size distribution of PBNPs immobilized on different chemical surfaces: (a) and (b) PBNPs-$NH_2(CH_2)_6S$-Au(111); (c) and (d) PBNPs-$OOC(CH_2)_5S$-Au(111); (e) and (f) PBNPs-$CH_3(CH_2)_5S$-Au(111). AFM images: 2 μm x 2 μm. The PBNP size distribution is based on statistic analysis of the particle height profiles in the AFM images, and at least 300 particles were used in each statistic analysis.

Main Parameters for ET and Electrocatalysis

Table 1. Comparison of the redox potential and population of -$NH_2(CH_2)_n$-. Scan rate 0.5 V s^{-1}.

Systems	Formal redox potential $E^{0'}$ (mV) vs. SCE	Rate constant K_s (S^{-1})	Normalized current density $10^{-4} j_{cat}$ (A/mol.M)
PBNPs-$H_2N(CH_2)_2S$-Au	149	1706	77
PBNPs-$H_2N(CH_2)_6S$-Au	154	1166	37
PBNPs-$H_2N(CH_2)_9S$-Au	152	599	25
PBNPs-$H_2N(CH_2)_{11}S$-Au	181	15	13
PBNPs-$H_2N(CH_2)_{16}S$-Au	177	0.4	0.9

Table 2. Comparison of the redox potential and population of -$COOH(CH_2)_n$-. Scan rate 0.5 V s^{-1}.

Systems	Formal redox potential $E^{0'}$ (mV) vs SCE	Rate constant K_s (S^{-1})	Normalized current density $10^{-3} j_{cat}$ (A/mol.M)
PBNPs-$OOC(CH_2)_2S$-Au	147	920	142
PBNPs-$OOC(CH_2)_5S$-Au	152	175	43
PBNPs-$OOC(CH_2)_9S$-Au	142	22	29
PBNPs-$OOC(CH_2)_{10}S$-Au	188	0.8	undetectable

Table 3. Comparison of the redox potential and population of -$CH_3(CH_2)_n$- . Scan rate 0.05 V s^{-1}.

Systems	Formal redox potential $E^{0'}$ (mV) vs SCE	Rate constant K_s (S^{-1})	Normalized current density $10^{-4} j_{cat}$ (A/mol.M)
PBNPs-$H_3C(CH_2)_2S$-Au	140	7.7	48
PBNPs-$H_3C(CH_2)_5S$-Au	144	2.5	29
PBNPs-$H_3C(CH_2)_9S$-Au	137	0.4	24
PBNPs-$H_3C(CH_2)_{11}S$-Au	125	0.05	undetectable

Conclusion We have demonstrated feasibility of tuning interfacial ET and electrocatalysis for redox-active nanoparticles by modification of the Au(111) electrode surfaces via surface self-assembly chemistry. The SAMs offer different surfaces with distinct chemical properties for immobilization of 6 nm inorganic hybrid PBNPs. PBNPs were stable on all the three types of surfaces, but display different ET and electrocatalytic efficiency. Surface interactions between the PBNP and SAM are mostly likely responsible for the present observations. The results appear to reflect the heterogeneous structures of the PBNP surfaces.

References

1. Ricci, F.; Palleschi, G. *Biosensor & Bioelectronics* **2005**, *21*, 389.
2. Chi, Q.; Zhang, J.; Andersen, J. E. T.; Ulstrup, J. *J. Phys. Chem. B* **2001**, *105*, 4669.
3. Chi, Q.; Farver, O.; Ulstrup, J. *Proc. Natl. Acad. Sci.USA* **2005**, *102*, 16203.